

Learning linear optical circuits with coherent states

T.J. Volkoff

*Theoretical Division, Los Alamos National Laboratory, Los Alamos, NM, USA. and
Quantum Science Center*

Andrew T. Sornborger

*CCS-3, Los Alamos National Laboratory, Los Alamos, NM, USA. and
Quantum Science Center*

We analyze the energy and training data requirements for supervised learning of an M -mode linear optical circuit by minimizing an empirical risk defined solely from the action of the circuit on coherent states. When the linear optical circuit acts non-trivially only on $k < M$ unknown modes (i.e., a linear optical k -junta), we provide an energy-efficient, adaptive algorithm that identifies the junta set and learns the circuit. We compare two schemes for allocating a total energy, E , to the learning algorithm. In the first scheme, each of the T random training coherent states has energy E/T . In the second scheme, a single random MT -mode coherent state with energy E is partitioned into T training coherent states. The latter scheme exhibits a polynomial advantage in training data size sufficient for convergence of the empirical risk to the full risk due to concentration of measure on the $(2MT - 1)$ -sphere. Specifically, generalization bounds for both schemes are proven, which indicate the sufficiency of $O(E^{1/2}M)$ training states ($O(E^{1/3}M^{1/3})$ training states) in the first (second) scheme.

I. INTRODUCTION

Spatially- or temporally-multiplexed linear optical circuits are the central components of devices that process photon-encoded quantum information and therefore play a vital role in photonic information processing [12, 37]. After the initial generation of nonclassical resource states using optical nonlinearities or heralded entanglement, a set of linear optical layers are responsible for constructing the complexity required for production of photonic or continuous-variable (CV) cluster states, which are the central resources for optical implementations of measurement-based quantum computation.

As an example of this structure, consider the Borealis device [26], in which 216 pulses (length τ) of single temporal mode CV squeezed states are sequentially routed through time-delay loops of length τ , 6τ , and 36τ . Three variable beamsplitters, situated where the respective time-delay loops meet the mainline, allow the application of a linear optical circuit, generating long-range entanglement between the temporal modes. Validation that this device indeed produces large scale nonclassical CV states with high modal photon occupation was key for demonstrating quantum supremacy for Gaussian boson sampling protocols implemented via the coupling of a photon number resolving detector to the Borealis linear optical circuit [26].

Additionally, recent demonstration of scalable, programmable, time-multiplexed, and universal 3-mode linear optical operations [46] provides evidence that linear optical modules can be successfully implemented in near-term photonic quantum neural networks.

Analogous to the problem of learning quantum k -juntas which act nontrivially on a k -qubit subregister [6], in this work, we define the problem of learning linear op-

tical k -juntas (k -LOJ), i.e., learning the modes on which a linear optical unitary acts nontrivially (the junta) and, potentially simultaneously, learning the action of the unitary on the junta modes. This problem is a specific example of methodology to characterize or certify the dynamical behavior of an optical circuit. Our approach to this problem consists of a hybrid quantum-classical algorithm utilizing coherent state inputs and CV SWAP tests [41] to compute and minimize an empirical risk function.

From a broader perspective, because each matrix element of a k -LOJ corresponds to a tunable physical parameter, statistical learning of k -LOJs as considered in the present work can be considered as a type of CV quantum process tomography, i.e., the task of obtaining classical estimates of CV quantum channels (including CV quantum state tomography) [9, 20, 23, 25, 29, 38, 47], for which specific methods have been introduced in the case of characterizing linear optical circuits [2, 7, 8, 14–16, 22, 28, 30, 31, 39]. These methods have not previously made use of hybrid quantum-classical algorithms.

We emphasize that learning the parameters of more general CV quantum neural networks [17] with the aim of compiling a target unitary dynamics (i.e., CV quantum compiling [42]) is generally less resource intensive than full quantum process tomography of the target unitary. This is because CV quantum compiling does not involve full classical characterization of all matrix elements of a target CV quantum circuit, but only learning an at-most-polynomial number of parameters that specify the ansatz CV quantum neural network. These parameters often take the form of the discrete structure specifications and interaction strengths.

Our use of coherent states as training data is motivated by the fact that linear optical unitaries have a transitive action on the set of isoenergetic coherent states. Further, information obtained from measurements in the overcom-

plete coherent state or generalized coherent state basis has been useful for CV quantum state tomography [35].

Statistical learning methods have been employed for classification of corrupted CV states from their approximate coherent state support (discretized Husimi q -function) [1]. However, our empirical risk minimization uses neither entangled states nor CV state tomography subroutines. It relies solely on distinguishing coherent states via the CV SWAP test. Because linear optical unitaries preserve total photon number, the precision of the CV SWAP test depends only on the energy of the training coherent states. We define two empirical risk minimization (ERM) settings, **ERM1** and **ERM2**, which differ in the way that the training coherent states are generated. An energetic modification to **ERM1**, called **ERM1'**, allows quantitative comparison of the two training state generation methods.

The respective generalization performances of the ERM settings are found to depend on the number of modes of the linear optical circuit and the energy (in addition to the training set size, as usual). In the ERM settings that we consider, the respective covering number generalization bounds are proven using McDiarmid's inequality (**ERM1**, **ERM1'**) and Lévy's lemma (**ERM2**). These bounds may find other applications in quantum machine learning utilizing cost functions defined on products of many spheres, or spheres of large dimension. The problem of using nonclassical states of light for learning linear optics in the same hybrid quantum-classical framework (or otherwise) is left to future work.

We work with a common notational framework for CV systems. The vector of canonical operators (quadratures) is $R = (q_1, \dots, q_M, p_1, \dots, p_M)^T$, where the components satisfy the Heisenberg canonical commutation relation $[R_i, R_j] = i\Omega_{i,j}$, and

$$\Omega = \begin{pmatrix} 0 & I \\ -I & 0 \end{pmatrix} \quad (1)$$

is the symplectic form on \mathbb{R}^{2M} . The photon number operator is $N_M := \frac{1}{2}R^T R$ with unique lowest eigenvector $|0\rangle^{\otimes M}$. A Heisenberg-Weyl coherent state is defined as $|x\rangle = D(x)|0\rangle^{\otimes M}$, where $D(x) = e^{-ix^T \Omega R}$, and the parameter x has the physical meaning of the mean vector of the coherent state, viz., $\langle R \rangle_{|x\rangle} = x$.

There is a one-to-one correspondence between a Gaussian unitary operation U and a symplectic matrix $T_U \in Sp(2M, \mathbb{R})$ which acts on the quadrature vector operator as

$$U^\dagger R U = T_U R. \quad (2)$$

The Euler decomposition for $Sp(2M, \mathbb{R})$ implies that a Gaussian circuit can always be written as a composition of squeezing operations followed by a linear optical unitary [4, 33] and, indeed, this is how NISQ circuits for Gaussian boson sampling are organized [3]. If U is a linear optical unitary, then $T_U \in O(2M) \cap Sp(2M, \mathbb{R}) = K(2M)$, the maximal compact subgroup of $Sp(2M, \mathbb{R})$.

II. LINEAR OPTICAL k -JUNTAS

The maximal compact subgroup $K(2M)$ is seen to be isomorphic to the unitary group $U(M)$ by noting that if $G = \text{Re}G + i\text{Im}G$, then

$$\begin{pmatrix} \text{Re}G & \text{Im}G \\ -\text{Im}G & \text{Re}G \end{pmatrix} \in K(2M) \quad (3)$$

and, conversely, that the $(1, 1)$ and $(1, 2)$ $M \times M$ blocks of any element of $K(2M)$ define the real and imaginary parts of an $M \times M$ unitary. However, due to connectivity and transmissivity restrictions in linear optical circuits, linear optical unitaries often do not change every element of a coherent state mean vector.

Definition 1. An orthogonal matrix in $O \in O(2M) \cap Sp(2M, \mathbb{R})$ is a linear optical k -junta (k -LOJ) if there exists a subspace $\mathcal{K} \subset \mathbb{R}^{2M}$ of dimension $2M - 2k$ and $T \in O(2k) \cap Sp(2k, \mathbb{R})$ such that $O = T \oplus I_{2M-2k}$.

This notion is straightforwardly related to the notion of quantum k -junta for linear optical unitaries [6, 44].

Lemma 1. If O is a k -LOJ and $U^\dagger R U = O R$, then there exists a set of M CV modes for which U is a quantum k -junta.

Proof. There is an isometric isomorphism from \mathbb{R}^{2M} to itself that takes the subspace \mathcal{K} in Definition 1 to the subspace spanned by $\{e_1, \dots, e_{2M-2k}\}$. Associate these $2M - 2k$ orthogonal directions in \mathbb{R}^{2M} with a vector of canonical operators $\hat{R}_{\mathcal{K}} = (q_1, p_1, \dots, q_{M-k}, p_{M-k})^T$, and complete this vector to a vector of canonical operators for an M -mode CV system $\hat{R} = \hat{R}_{\mathcal{K}^c} \oplus \hat{R}_{\mathcal{K}}$. Then the unitary U associated with O acts as identity on $\hat{R}_{\mathcal{K}}$, i.e., $U = \mathbb{I}_{\mathcal{K}} \otimes U'$ for unitary U' on $\mathcal{H}^{\otimes k}$. \square

In practice, a circuit-based CV quantum information processing protocol is defined with respect to a predefined set of M modes. A linear optical unitary that is a quantum k -junta with respect to these modes is then associated with k -LOJ in which the subspace \mathcal{K} is defined by a $(M - k)$ -subset of the modes. We now fix the set of M CV modes and restrict our consideration to a k -LOJ with \mathcal{K} having an orthonormal basis indexed by a subset of $[M]$.

III. COHERENT STATE ERM

Before detailing a variational ERM algorithm for learning k -LOJ, we discuss features of the ERM problem for general linear optical unitaries. Consider a set of training coherent states $S = \{|x^{(j)}\rangle\}_{j=1}^T$, $x^{(j)} \in \mathbb{R}^{2M}$, and empirical risk function for learning a target linear optical unitary U

$$\hat{C}_S(V) = \frac{1}{4T} \sum_{j=1}^T \|(\mathcal{U} - \mathcal{V})(|x^{(j)}\rangle)\langle x^{(j)}|\|_1^2 \quad (4)$$

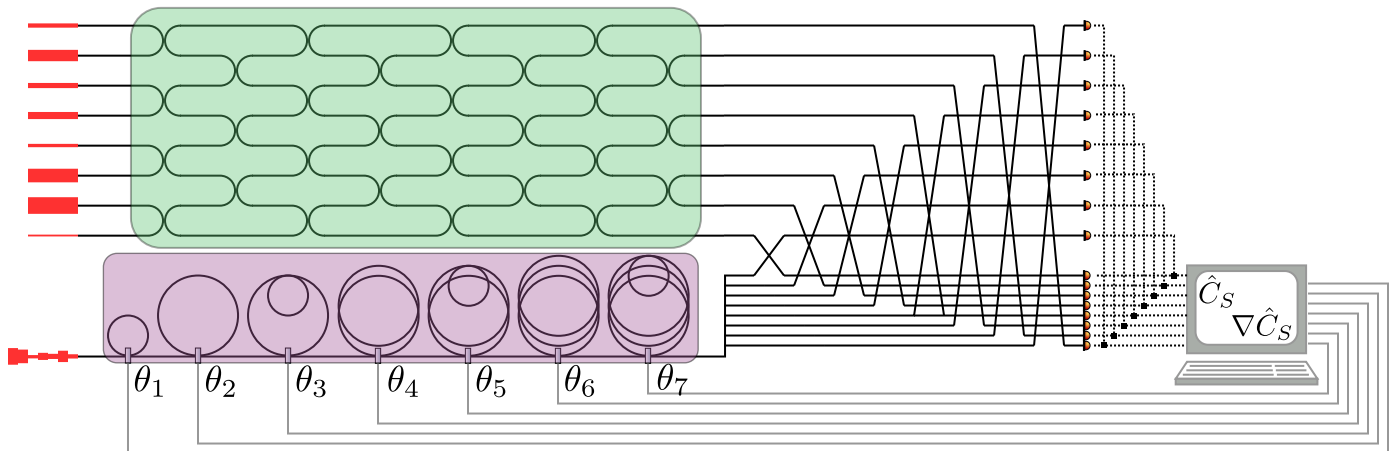


FIG. 1: A method for $T = 1$ empirical risk function calculation by CV SWAP test and classical optimization algorithm. A random training coherent state is injected into spatial modes of the target linear optical circuit U (green) and temporal modes of the time-delay multiplexed circuit $V(\theta)$ (pink). The rectangular decomposition is used to signify U . The τ -loop and 2τ -loop time-multiplexed circuit with programmable beamsplitters allows to implement arbitrary linear optical ansatz circuit $V(\theta)$ on $M = 8$ temporal modes. The 8τ signal from $V(\theta)$ is spatially demultiplexed and the CV SWAP test (beamsplitter network and photon counting) is performed.

where $V = V(\theta)$ is a linear optical unitary parameterized by θ and we denote a unitary channel by $\mathcal{U}(\cdot) := U(\cdot)U^\dagger$ for any unitary U . The empirical risks can be computed by using parity data from photon number counting measurement on corresponding pairs of modes of $U|x\rangle$ and $V|x\rangle$ as in the CV SWAP test, which has known energy cost when coherent state inputs are used [41]. Minimization of (4) in the case of a single training coherent state is drawn in Fig. 1, in which a target unitary (shown in a generic rectangular decomposition) is learned by updating the variable beamsplitters of a time-delay-multiplexed circuit. It is possible to use commonly implemented circuit architectures for $V(\theta)$, such as triangular decomposition or rectangular decomposition, but in the numerical optimizations in this work, we directly optimize over matrix elements so as to circumvent parametrization-dependent challenges in optimization. Unlike the case for unitary matrices in the computational basis on discrete-variable quantum systems, the matrix elements of V are directly tunable because they are simply the couplings between field quadratures.

We will consider two ways of enforcing an energy constraint on the training set S . In **ERM1**, $\|x^{(j)}\| = \sqrt{2E}$ for all j , so each training coherent state has energy E . In **ERM2**, one considers T projections of an MT -mode coherent state $|x\rangle$ to the respective M -mode subsystems using the projections $P_j : \mathbb{R}^{2MT} \rightarrow \mathbb{R}^{2M}$ with $P_j x = (x_{2M(j-1)+1}, \dots, x_{2Mj})$, $j = 1, \dots, T$. One defines the local M -mode coherent states by $|x^{(j)}\rangle = |P_j x\rangle$. Taking $\|x\| = \sqrt{2E}$, the training set S has total energy E , regardless of its size. Note that for $T > 1$, **ERM1** has strictly greater total energy than **ERM2**; later we will introduce a modification to **ERM1**, called **ERM1'**, in which the training data set has total energy equal to

that of **ERM2**. These energy-constrained empirical risk functions correspond to empirical risk minimization tasks with serial and parallel training coherent state sources, respectively. When variationally learning a linear optical unitary, the empirical risk serves as an estimate of the full risk

$$C_{\text{ERM1}}(V) := \frac{1}{4} \int_{S^{2M-1}} \|(\mathcal{U} - \mathcal{V})(|x\rangle\langle x|)\|_1^2$$

$$C_{\text{ERM2}}(V) := \frac{1}{4} \int_{S^{2MT-1}} \|(\mathcal{U} - \mathcal{V})(|P_1 x\rangle\langle P_1 x|)\|_1^2 \quad (5)$$

where both integrals are over the uniform measure on the respective sphere (of radius $\sqrt{2E}$ for **ERM1** and **ERM2**). Note that $C_{\text{ERM2}}(V)$ depends on T because the local training coherent state $|P_j x\rangle$ in the j -th subsystem is obtained from a MT -mode coherent state. The following chain of inequalities shows that each term in the sum (4) has a simple upper bound in terms of the orthogonal matrices associated to U and V , and the energy constraint:

$$\begin{aligned} \frac{1}{2} \|(\mathcal{U} - \mathcal{V})|x\rangle\langle x|\|_1 &= \sqrt{1 - |\langle x|U^\dagger V|x\rangle|^2} \\ &= \sqrt{1 - e^{-\frac{1}{2}x^T(O_U - O_V)^T(O_U - O_V)x}} \\ &\leq \sqrt{1 - e^{-\frac{1}{2}\|x\|^2\|O_U - O_V\|^2}} \\ &\leq \sqrt{E}\|O_U - O_V\| \end{aligned} \quad (6)$$

with $\|x\| = \sqrt{2E}$. This fact implies Lipschitz continuity of the empirical risk and the full risk in both settings.

Lemma 2. *Let W and V be linear optical unitaries such*

that $\|O_W - O_V\| \leq \frac{\epsilon}{\sqrt{E}}$. Then,

$$\begin{aligned} |\hat{C}_S(W) - \hat{C}_S(V)| &\leq \epsilon \text{ with probability } 1 \\ |C_{\mathbf{ERM1}}(W) - C_{\mathbf{ERM1}}(V)| &\leq \epsilon. \end{aligned} \quad (7)$$

If $\|O_W - O_V\| \leq \epsilon \sqrt{\frac{2MT-1}{E(2M+1)}}$, then

$$|C_{\mathbf{ERM2}}(W) - C_{\mathbf{ERM2}}(V)| \leq \epsilon. \quad (8)$$

Proof. We show the first inequality; the proof of the second is the same, replacing the discrete measure over training states with the uniform measure.

$$\begin{aligned} &|\hat{C}_S(W) - \hat{C}_S(V)| \\ &\leq \frac{1}{T} \sum_{j=1}^T \left| |\langle x^{(j)} | UW^\dagger | x^{(j)} \rangle|^2 - |\langle x^{(j)} | UV^\dagger | x^{(j)} \rangle|^2 \right| \\ &\leq \frac{1}{2} \max_j \|W |x^{(j)}\rangle \langle x^{(j)}| W^\dagger - V |x^{(j)}\rangle \langle x^{(j)}| V^\dagger\|_1 \\ &\leq \epsilon \end{aligned} \quad (9)$$

where we note that for **ERM2**, $\|x^{(j)}\| \leq \sqrt{2E}$ trivially because $\|x\| = \sqrt{2E}$. The first inequality uses the definition of trace distance for pure states and the triangle inequality, the second inequality is standard (Eq. (9.96) of [45]), the third inequality is (6).

For **ERM2** the Lipschitz constant of the cost function is smaller. Note that

$$\begin{aligned} &|C_{\mathbf{ERM2}}(W) - C_{\mathbf{ERM2}}(V)| \leq \\ &\int_{S^{2MT-1}} |\langle P_1 x | UW^\dagger | P_1 x \rangle|^2 - |\langle P_1 x | UV^\dagger | P_1 x \rangle|^2 \\ &\leq \frac{1}{\sqrt{2}} \|O_W - O_V\| \int_{S^{2MT-1}} \|P_1 x\|. \end{aligned} \quad (10)$$

Carrying out the integral using the marginal in (12) and Gautschi's inequality gives that the last line is upper bounded by $\|O_W - O_V\| \sqrt{E(2M+1)/(2MT-1)}$. \square

We note that the integrals defining the full risks (5) do not have closed form expressions, but can be approximated from series expansions, similar to hypergeometric functions of matrix argument [18]. For instance, $1 - C_{\mathbf{ERM1}}(V)$ is given by

$$2E^{2M-1} \sum_{i_1, \dots, i_{2M}=0}^{\infty} \frac{\prod_{j=1}^{2M} \frac{1}{i_j!} \left(-\frac{\kappa_j^2}{2}\right)^{i_j} \Gamma(i_j + \frac{1}{2})}{\Gamma(M + \sum_{j=1}^{2M} i_j)}. \quad (11)$$

where $\kappa_1, \dots, \kappa_{2M}$ are the singular values of $O_U - O_V$.

To determine whether numerical minimization of (4) successfully learns U , in both Figs. 2a and 2b we observe that below the critical value $T = M$, minimization of (4) fails to return a $W \in K(2M)$ that approximates the target O_U closely in Frobenius norm. At $T = M$, we observe

a transition to successful learning of U (if success is characterized by an appropriate value of the Hilbert-Schmidt distance). This transition is explained by the fact that a $2M \times 2M$ symplectic orthogonal matrix is a function of two $M \times M$ block submatrices, so M linearly independent training coherent states are sufficient to make $C_{\mathbf{ERM1}(2)}$ a faithful cost function (almost everywhere with respect to the measure governing the training set S), i.e., the unique global minimum occurs for $V = U$.

However, even when the empirical risk is almost always faithful (which is the case for $T \geq M$), the performance of the minimization algorithm depends on how the energy scales with the number of modes, due to the energy-dependent barren plateau phenomenon [43]. Specifically, when the energy of a multimode coherent state scales at least linearly with the number of modes, the expected magnitude of the gradient of the empirical risk exponentially decreases to zero with respect to increasing M , rendering gradient-descent-based minimization algorithms ineffective. This energy-dependent barren plateau phenomenon is the cause of the reduced effectiveness of the learning algorithm **ERM1** for large energies. For example, in Fig. 2a, the minimization is successful for $E = 4$, but the minimization is rarely successful for $E = 16$.

To see how this problem is lessened for **ERM2**, we appeal to the marginal probability density of each of the T M -mode coherent states comprising a training set in **ERM2**. Without loss of generality [27],

$$p(x^{(1)}) \propto \frac{\theta(2E - \|x^{(1)}\|^2)}{(2E)^{MT-1}} (2E - \|x^{(1)}\|^2)^{M(T-1)-1}. \quad (12)$$

From this marginal density, one finds that the expected energy of each of the individual training coherent states $|x^{(i)}\rangle$ in **ERM2** is E/T . If the energy E is chosen to scale linearly with M , then increasing T reduces the impact of the exponential factor that causes the energy-dependent barren plateau phenomenon, which eases optimization [43]. In fact, the data in Fig. 2b is closely replicated by the scheme of **ERM1** modified by requiring that each training coherent state have energy E/T , i.e., $\|x^{(i)}\| = \sqrt{2E/T}$. We will call this modified scheme **ERM1'**. However, in the next section, we see that concentration of $C_{\mathbf{ERM2}}$ on the sphere embedded in \mathbb{R}^{2MT} causes an increased rate of convergence to the associated risk function (with respect to T) compared to $C_{\mathbf{ERM1}}$.

Before carrying out an analysis of generalization bounds for the empirical risk minimization settings, we first introduce an energy-efficient method for learning a k -LOJ. Specifically, the target orthogonal matrix is promised to be a k -LOJ, but the junta set $J \subset [M]$, $|J| = k$ is unknown. The energy-efficient adaptive method in Algorithm 1 is based on the fact that if the subset J were perfectly known, then it would be wasteful to use training coherent states that are non-vacuum on the J^c modes. The eventual success of Algorithm 1 is predicated on the success of the empirical risk minimization when T is at least the size of the junta set, which

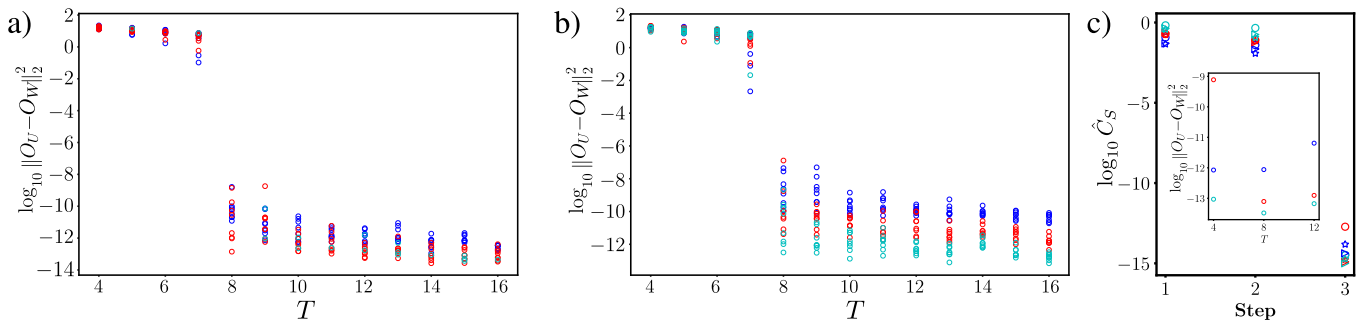


FIG. 2: Empirical risk minimization for a uniform random 8-mode target linear optical unitary, U , with 8 uniformly random coherent state training datasets of size $T \in \{4, \dots, 16\}$. If a training dataset did not result in finding a W such that $\hat{C}_S(W) < 10^{-7}$, it was not shown. Quality of the minimization output is quantified by $\|O_U - O_W\|_2^2$. a) (**ERM1**) Blue, $E = 1$; Red, $E = 4$; Cyan $E = 16$. **ERM1** failed to obtain a minimum for $T < 8$. This is expected since the empirical risk is not faithful for a smaller training dataset. b) (**ERM2**) Blue, $E = 1$; Red, $E = 4$; Cyan $E = 16$. The constraint $\|V^\dagger V - \mathbb{I}_M\|_2^2 \leq 10^{-6}$ was enforced on the variational matrix V during this simulated ERM to ensure approximate unitarity. Note that many more cyan ($E = 16$) datapoints are found, indicating that **ERM2** has a more favorable landscape for optimization relative to **ERM1**. c) \log_{10} of the **ERM2** empirical risk minimal value for learning a single, random 4-LOJ on $M = 8$ modes using Algorithm 1 ($J = \{3, 4, 5, 8\}$ for this target unitary). Circles are $T=4$, triangles are $T = 8$, stars are $T = 12$. Note that $T \geq 4$ is necessary for faithful empirical risk for a target 4-LOJ. The junta size determines the number of steps that the algorithm takes; here, the junta size is 4 and therefore 3 steps of the algorithm suffices. Inset shows distance of output O_W from O_U after third step for various T . We see that the distance of the learned matrix to the target matrix is smaller for higher energy.

can be demonstrated utilizing an analysis similar to that discussed above for Figs. 2a, b.

Algorithm 1 finds the junta set J and learns the target k -LOJ using $O((M+k)^2)$ minimizations of a faithful empirical risk, e.g., \hat{C}_S defined by a training set of size at least k . In the pseudocode for Algorithm 1, we have suppressed the subroutine generating the training states for empirical risk minimization with the 2-LOJ ansatz defined by members of \mathcal{J}_2 , the 3-LOJ ansatz defined by members of \mathcal{J}_3 , etc. To define this subroutine, first note that at the iteration defined by \mathcal{J}_k , one should use training sets of size $T \geq k$ so that the empirical risk function is faithful for learning k -LOJ and, therefore, so that the algorithm can in principle terminate. Then, to utilize the k training states in an energy-efficient way within **ERM2**, note that identifying a minimal value c_2 requires an energy at least E_2 for each of the trials in \mathcal{J}_2 , which depends on the specific implementation (one can see this by noting that, e.g., $\hat{C}_S \rightarrow 1$ for $\|x\| \rightarrow 0$). Similarly, in a general iteration j , identifying the minimal value c_j requires a minimal total energy E_j . Within the scheme **ERM2**, this procedure consumes energy at most $\binom{M}{2}E_2 + (M-2)E_3 + \dots + (M-k+1)E_k$. Numerical data obtained by applying Algorithm 1 to a random $M = 8$ mode 4-LOJ is shown in Fig. 2c).

Note that there are many non-generic instances of U (but commonly encountered in actual devices) where this algorithm would terminate in the first junta set update. For instance, consider U being a tensor product of generalized beamsplitters on modes $(1, 2)$, $(3, 4)$, $(M, M-1)$. After the junta set update, one would conclude that not

only is the junta set $J = [M]$, but the U is given by $\bigotimes_{j=1}^{M-1} V^{(j,j+1)}(\alpha_c^{(i,j)})$ to high accuracy. In Algorithm 1, we start with pairs of modes because one can consider generalized beamsplitters as a fundamental linear optical element, which subsumes the case of a tensor product of single-mode phase shifts. Strictly speaking, the numerical precision of the optimization algorithm will allow to identify a mode set $J \cup \{l\}$ achieving the minimal value c_2, c_3 , etc., so there should be a small finite tolerance on what value is considered “minimal” so as not to do more ERM iterations than needed. It should be noted that the junta set updates in Algorithm 1 do not make use of quantum coherence. Introducing a discrete variable quantum register which controls the junta set updating procedure and carrying out, e.g., Grover’s algorithm for unstructured search, on that register could result in learning U after sublinear (in M) ERM runs.

Finally, we note that there are alternative algorithms that allow to identify the junta set J , but without learning the target k -LOJ. In Ref. [6], the junta set of a multiqubit unitary is determined with high probability by sampling its Pauli spectrum using the Choi state of the unitary. Since CV systems do not have an analog of the Pauli spectrum, a different quantum algorithm is required. In the case of finding the junta set for k -LOJ, the fact that linear optical unitaries preserve the set of coherent states allows a semiclassical algorithm utilizing only pure coherent states. We assume preparation of the $4M^2$ -mode coherent state

$$(U|x\rangle_A \otimes |x\rangle_B)^{\otimes M} \otimes (U|y\rangle_C \otimes |y\rangle_D)^{\otimes M} \quad (13)$$

Algorithm 1 k -LOJ learning with adaptive linear optical ansatze

```

1: Given:  $k$ -LOJ  $O_U$  with unknown  $k$  and junta set  $J$ 
2:  $J = \emptyset$ 
3:  $\mathcal{J}_2 = \{\{i, j\} \subset [M] : i < j\}$ 
4: Ansatz  $V^{i,j}(\alpha)$  acts nontrivially on modes  $\{i, j\}$ . Compute  $\min_{\alpha} \hat{C}_S(V^{i,j}(\alpha))$  for all  $\{i, j\} \in \mathcal{J}_2$  and return the minimal value  $c_2$ , which occurs for mode pairs  $\{i^{(1)}, j^{(1)}\}, \{i^{(2)}, j^{(2)}\}, \dots$ 
5:  $J \leftarrow \cup_{\ell} \{i^{(\ell)}, j^{(\ell)}\}$ 
6: if  $c_2 < 10^{-10}$  then
7:   Return  $J$  and  $\bigotimes_{\ell} V^{\{i^{(\ell)}, j^{(\ell)}\}}(\alpha_c^{\{i^{(\ell)}, j^{(\ell)}\}})$ 
8: else if  $c_2 \geq 10^{-10}$  then
9:    $\mathcal{J}_3 = \{J \cup \{l\} \subset [M] : l \notin J\}$ 
10:  Ansatz  $V^{J \cup \{l\}}(\beta)$  acts nontrivially on modes  $J \cup \{l\}$ . Compute  $\min_{\beta} \hat{C}_S(V^{J \cup \{l\}}(\beta))$  for all  $J \cup \{l\} \in \mathcal{J}_3$  and return the minimal value  $c_3$ , which occurs for mode sets  $J \cup \{l^{(1)}\}, J \cup \{l^{(2)}\}, \dots$ 
11: end if
12:  $J \leftarrow J \cup_{\ell} \{i^{(\ell)}\}$ 
13: if  $c_3 < 10^{-10}$  then
14:   Return  $J$  and  $\bigotimes_{\ell} V^{J \cup \{i^{(\ell)}\}}(\beta_c^{J \cup \{i^{(\ell)}\}})$ 
15: else if  $c_3 \geq 10^{-10}$  then
16:    $\mathcal{J}_4 = \{J \cup \{l\} \subset [M] : l \notin J\}$ 
17:  Ansatz  $V^{J \cup \{l\}}(\gamma)$  acts nontrivially on modes  $J \cup \{l\}$ . Compute  $\min_{\gamma} \hat{C}_S(V^{J \cup \{l\}}(\gamma))$  for all  $J \cup \{l\} \in \mathcal{J}_4$  and return the minimal value  $c_4$ , which occurs for mode sets  $J \cup \{l^{(1)}\}, J \cup \{l^{(2)}\}, \dots$ 
18: end if
19:  $J \leftarrow J \cup_{\ell} \{i^{(\ell)}\}$ 
20: if  $c_4 < 10^{-10}$ 
21:   Return  $J$  and  $\bigotimes_{\ell} V^{J \cup \{i^{(\ell)}\}}(\gamma_c^{J \cup \{i^{(\ell)}\}})$ 
22: Etc.

```

where $A = (A_1, \dots, A_M)$ is an M -mode CV system (similarly for B, C, D), and $P_j x \neq \lambda P_j y$ for any $\lambda \in \mathbb{R}$, where P_j is the projector to the j -th component of a vector in \mathbb{R}^{2M} . The above state is equal to

$$\bigotimes_{j=1}^M \left[|P_j O_U x\rangle \langle P_j O_U x|_{A_j} \otimes |P_j x\rangle \langle P_j x|_{B_j} \otimes |P_j O_U y\rangle \langle P_j O_U y|_{C_j} \otimes |P_j y\rangle \langle P_j y|_{D_j} \right]. \quad (14)$$

For each $j \subset [M]$, the CV SWAP test is carried out on (14) between modes A_j and B_j and between modes C_j and D_j [41]. If both succeed, the mode j is appended to the complement of the junta set. This procedure is repeated according to the energy-dependent complexity results of [41], producing the junta set to a desired accuracy.

IV. GENERALIZATION BOUNDS

In quantum machine learning with few training data, and, specifically in the task of learning quantum dynamics, the empirical risk often does not define a faithful cost function. Generalization bounds allow to bound the probability that the value of the empirical risk differs by some small amount from the value of the full risk. Obtaining the minimal value of the full risk on a hypothesis unitary guarantees that the dynamics has been learned exactly. When proving generalization bounds for full risk functions that are defined via expectation values of observables that are only constrained roughly (e.g., by their operator norm), the concentration inequality used to derive the generalization bound must be correspondingly general. For instance, in [5] the only quantity constraining the empirical risk is the norm of the observable defining the loss function, so the relevant concentration inequalities are for independent, identically distributed random variables in an interval defined by that norm. Since the empirical risk functions in this paper are functions of high-dimensional sphere-valued random variables with the sphere radius determined by the energy and risk minimization setting, concentration on the sphere is the relevant concept for determining the convergence rate of the empirical risk to the full risk.

Let X be a random variable taking values on the D -sphere in \mathbb{R}^{D+1} with radius R , and let the distribution of X have uniform density on the sphere. Consider the Gaussian function

$$f(X) = e^{-\frac{1}{2} X^T L(U, V) X} \quad (15)$$

where $L(U, V) := (O_U - O_V)^T (O_U - O_V)$ is a positive, symmetric matrix. The restriction of the function (15) to the D -sphere of radius R is κ -Lipschitz where

$$\kappa \leq \|L(U, V)\| R e^{-\lambda_{\min}(L(U, V))E} \leq R \|L(U, V)\|. \quad (16)$$

The concentration of a function, f , of a sphere-valued random variable about its expectation, $E(f)$, is related to the Lipschitz constant, κ , through Lévy's lemma [13]

$$P(|f(X) - E(f(X))| \geq \eta) \leq 2e^{-\frac{C_1(D+1)\eta^2}{\kappa^2}}. \quad (17)$$

The generalization bounds for learning a linear optical unitary that appear in Theorem 1 indicate a qualitative difference in the size of the coherent state training set required for convergence of **ERM1** and **ERM2** learning protocols.

Theorem 1. (*Generalization bounds for learning O_U*) *Let $V(\theta_S)$ be the unitary minimizing (4) for each training set S . Then, with $C_1 = (9\pi^3 \ln 2)^{-1}$, the following bound holds with probability at least $1 - \delta$ over training sets S*

of energy E and size T

$$\begin{aligned} & |C_{\mathbf{ERM2}}(V(\theta_S)) - \hat{C}_S(V(\theta_S))| \\ & < \sqrt{\frac{16EM \log 6\sqrt{C_1MT^3}}{C_1T^3} + \frac{16E \log \frac{2}{\delta}}{C_1MT^3}} \\ & + 2\sqrt{\frac{E}{C_1MT^3}}. \end{aligned} \quad (18)$$

if S satisfies the energy constraint in **ERM2**, and

$$\begin{aligned} & |C_{\mathbf{ERM1}}(V(\theta_S)) - \hat{C}_S(V(\theta_S))| \\ & < \sqrt{\frac{32EM^2 \log 6\sqrt{T}}{T} + \frac{32E \log \frac{2}{\delta}}{T}} \\ & + 2\sqrt{\frac{E}{T}} \end{aligned} \quad (19)$$

if S satisfies the energy constraint in **ERM1**.

Proof. We first prove (18) because it makes use of Lévy's lemma. Let $\mathcal{N}_{\epsilon/\sqrt{E}} = \{g_j\}_j$ be an ϵ/\sqrt{E} cover of $O(2M)$. Consider a fixed training set S . From Lemma 2, it follows that there is a $g \in \mathcal{N}_{\epsilon/\sqrt{E}}$ such that (with probability 1 over S)

$$|\hat{C}_S(g) - C(g)| - |\hat{C}_S(V(\theta_S)) - C(V(\theta_S))| \leq 2\epsilon. \quad (20)$$

From this, it follows that

$$\begin{aligned} & P_S \left[|\hat{C}_S(V(\theta_S)) - C(V(\theta_S))| \geq \eta + 2\epsilon \right] \\ & \leq P_S \left[\exists g \in \mathcal{N}_{\epsilon/\sqrt{E}} : |\hat{C}_S(g) - C(g)| \geq \eta \right] \end{aligned} \quad (21)$$

because if the event on the left hand side holds and $|\hat{C}_S(g) - C(g)| < \eta$ for all $g \in \mathcal{N}_{\epsilon/\sqrt{E}}$, then (20) implies that $V(\theta_S)$ cannot be in an ϵ/\sqrt{E} neighborhood of any g , which is a contradiction. For **ERM2**, the Lipschitz constant in Levy's lemma (17) is upper bounded using

$$\max_{\substack{x \in \mathbb{R}^{2MT} \\ \|x\| = \sqrt{2E}}} \|\nabla \hat{C}_S(g)\| \leq \frac{\sqrt{2E}}{T} \|L(U, g)\| \leq \frac{4\sqrt{2E}}{T}, \quad (22)$$

where $L(U, g)$ is defined below (15). Applying the union bound gives that the right hand side of (21) is

$$\begin{aligned} & \leq 2|\mathcal{N}_{\frac{\epsilon}{\sqrt{E}}}| e^{-\frac{C_1MT^3\eta^2}{16E}} \\ & \leq 2 \left(\frac{6\sqrt{E}}{\epsilon} \right)^{M^2} e^{-\frac{C_1MT^3\eta^2}{16E}}. \end{aligned} \quad (23)$$

Taking

$$\eta = \sqrt{\frac{16EM \log \frac{6\sqrt{E}}{\epsilon}}{C_1T} + \frac{16E \log \frac{2}{\delta}}{C_1MT}} \quad (24)$$

gives that the right hand side of (21) is upper bounded by δ . Taking $\epsilon = \sqrt{\frac{E}{C_1MT}}$ so that η and 2ϵ have the same scaling with T , it follows that the event (18) holds with probability greater than $1 - \delta$.

To prove (19) one cannot use Lévy's lemma because \hat{C}_S is defined on a product of spheres $(S^{2M-1})^{\times T}$ instead of a single sphere. However, McDiarmid's inequality [40] is suitable for analyzing concentration of functions of i.i.d. random variables when an upper bound on the Lipschitz constant of the function is available. Under the assumptions of **ERM1**, one notes that

$$\max_{\substack{(x^{(1)}, \dots, x^{(T)}) \\ \|x^{(1)}\| = \dots = \|x^{(T)}\| = \sqrt{2E}}} \|\nabla \hat{C}_S(g)\| \leq 4\sqrt{2E}. \quad (25)$$

Therefore, due to fact that \hat{C}_S is a symmetric function on $(S^{2M-1}(\sqrt{2E}))^{\times T}$, the difference between \hat{C}_S evaluated at $(x^{(1)}, \dots, x^{(j)}, \dots, x^{(T)})$ and \hat{C}_S evaluated at $(v^{(1)}, \dots, v^{(j)}, \dots, v^{(T)})$ for any $j \in [T]$ is upper bounded by

$$\frac{\|L(U, g)\| \sqrt{2E}}{T} \|x^{(j)} - v^{(j)}\| \leq \frac{4E \|L(U, g)\|}{T}. \quad (26)$$

Applying McDiarmid's inequality and the union bound gives that the right hand side of (21) is now upper bounded by

$$2 \left(\frac{6\sqrt{E}}{\epsilon} \right)^{M^2} e^{-\frac{\eta^2 T}{32E}}. \quad (27)$$

Taking

$$\eta^2 = \frac{32EM^2 \log \frac{6\sqrt{E}}{\epsilon}}{T} + \frac{32E \log \frac{2}{\delta}}{T} \quad (28)$$

to get the $1 - \delta$ guarantee, and taking $\epsilon = \sqrt{\frac{E}{T}}$ gives the stated generalization bound. \square

To prove a generalization bound in the modified scheme **ERM1'**, which has the same total energy of the training set S as **ERM2**, one should follow the proof of (19) using McDiarmid's inequality, but the right hand side of (25) should be replaced by $4\sqrt{\frac{2E}{T}}$ owing to the $\|x^{(i)}\| = \sqrt{2E/T}$ constraint. One obtains that $T = O(M\sqrt{E})$ training states are sufficient for generalization.

V. DISCUSSION

The importance of linear optical circuits for photonic quantum information processing is indicated by the fact that techniques for automated quantum experiment design use linear optical circuits as primary examples and

testbeds [11, 19, 32]. In the present work, empirical risks for learning linear optical k -juntas are defined and calculated using coherent state training datasets with a fixed distribution of energy. Analysis of empirical risks defined by general energy-constrained CV Gaussian training states would not only allow optically non-classical training states, but could also extend the learning setting to include an entangled memory register [34, 42]. Improvements to sample complexity of learning linear optics are expected in this setting, following physically from the optimal sensitivity of non-classical CV Gaussian states to optical phase shifts under a mean energy constraint [24].

In terms of practical implementation, we consider **ERM2** to be well-suited to the scenario when the target linear optical circuit U is accessible in parallel by distributing T M -mode probe states. In contrast, **ERM1** or **ERM1'** seem more relevant if access to the unitary is scarce, e.g., in time. Regardless of the setting, we envision the training coherent states being generated by a circuit of random generalized beamsplitters applied to parent beam pulses. Lastly, we note that Algorithm 1 can be

made both more energy and sample-efficient if a restriction to a specific hypothesis class of ansätze $V(\theta)$ is made (even probabilistically, as would be relevant if a sharper prior on the target linear optical unitary is known). In these cases, it is also possible that more refined learning algorithms for linear optical circuits [10, 21, 36] could be applied in lieu of Algorithm 1.

ACKNOWLEDGMENTS

The authors thank Lukasz Cincio, Y. Subaşı, and Z. Holmes for useful discussions. This work was supported by the Quantum Science Center (QSC), a National Quantum Information Science Research Center of the U.S. Department of Energy (DOE). Los Alamos National Laboratory is managed by Triad National Security, LLC, for the National Nuclear Security Administration of the U.S. Department of Energy under Contract No. 89233218CNA000001.

-
- [1] Shah Nawaz Ahmed, Carlos Sánchez Muñoz, Franco Nori, and Anton Frisk Kockum. Classification and reconstruction of optical quantum states with deep neural networks. *Phys. Rev. Res.*, 3:033278, Sep 2021. doi:10.1103/PhysRevResearch.3.033278. URL <https://link.aps.org/doi/10.1103/PhysRevResearch.3.033278>.
- [2] Aamir Anis and A I Lvovsky. Maximum-likelihood coherent-state quantum process tomography. *New Journal of Physics*, 14(10):105021, oct 2012. doi:10.1088/1367-2630/14/10/105021. URL <https://dx.doi.org/10.1088/1367-2630/14/10/105021>.
- [3] J. M. Arrazola, V. Bergholm, K. Brádler, T. R. Bromley, M. J. Collins, I. Dhand, A. Fumagalli, T. Gerrits, A. Goussev, L. G. Helt, J. Hundal, T. Isacsson, R. B. Israel, J. Izaac, S. Jahangiri, R. Janik, N. Killoran, S. P. Kumar, J. Lavoie, A. E. Lita, D. H. Mahler, M. Menotti, B. Morrison, S. W. Nam, L. Neuhaus, H. Y. Qi, N. Quesada, A. Reppingon, K. K. Sabapathy, M. Schuld, D. Su, J. Swinerton, A. Száva, K. Tan, P. Tan, V. D. Vaidya, Z. Vernon, Z. Zabaneh, and Y. Zhang. Quantum circuits with many photons on a programmable nanophotonic chip. *Nature*, 591(7848):54–60, Mar 2021. ISSN 1476-4687. doi:10.1038/s41586-021-03202-1.
- [4] Arvind, B. Dutta, N. Mukunda, and R. Simon. The real symplectic groups in quantum mechanics and optics. *Pramana*, 45(6):471–497, Dec 1995. ISSN 0973-7111. doi:10.1007/BF02848172.
- [5] Matthias C. Caro, Hsin-Yuan Huang, M. Cerezo, Kunal Sharma, Andrew Sornborger, Lukasz Cincio, and Patrick J. Coles. Generalization in quantum machine learning from few training data. *Nature Communications*, 13(1):4919, Aug 2022. ISSN 2041-1723. doi:10.1038/s41467-022-32550-3. URL <https://doi.org/10.1038/s41467-022-32550-3>.
- [6] Thomas Chen, Shivam Nadimpalli, and Henry Yuen. Testing and learning quantum juntas nearly optimally. *arXiv preprint arXiv:2207.05898*, 2022.
- [7] Ish Dhand, Abdullah Khalid, He Lu, and Barry C Sanders. Accurate and precise characterization of linear optical interferometers. *Journal of Optics*, 18(3):035204, feb 2016. doi:10.1088/2040-8978/18/3/035204. URL <https://dx.doi.org/10.1088/2040-8978/18/3/035204>.
- [8] Ilya A Fedorov, Aleksey K Fedorov, Yury V Kurochkin, and A I Lvovsky. Tomography of a multimode quantum black box. *New Journal of Physics*, 17(4):043063, apr 2015. doi:10.1088/1367-2630/17/4/043063. URL <https://dx.doi.org/10.1088/1367-2630/17/4/043063>.
- [9] Jaromír Fiurášek. Continuous-variable quantum process tomography with squeezed-state probes. *Phys. Rev. A*, 92:022101, Aug 2015. doi:10.1103/PhysRevA.92.022101. URL <https://link.aps.org/doi/10.1103/PhysRevA.92.022101>.
- [10] Fulvio Flamini, Nicolò Spagnolo, Niko Viggianiello, Andrea Crespi, Roberto Osellame, and Fabio Sciarrino. Benchmarking integrated linear-optical architectures for quantum information processing. *Scientific Reports*, 7(1):15133, Nov 2017. ISSN 2045-2322. doi:10.1038/s41598-017-15174-2. URL <https://doi.org/10.1038/s41598-017-15174-2>.
- [11] Xuemei Gu, Manuel Erhard, Anton Zeilinger, and Mario Krenn. Quantum experiments and graphs ii: Quantum interference, computation, and state generation. *Proceedings of the National Academy of Sciences*, 116(10):4147–4155, 2019. doi:10.1073/pnas.1815884116. URL <https://www.pnas.org/doi/abs/10.1073/pnas.1815884116>.
- [12] Nicholas C. Harris, Jacques Carolan, Darius Bunandar, Mihika Prabhu, Michael Hochberg, Tom Baehr-

- Jones, Michael L. Fanto, A. Matthew Smith, Christopher C. Tison, Paul M. Alsing, and Dirk Englund. Linear programmable nanophotonic processors. *Optica*, 5(12):1623–1631, Dec 2018. doi:10.1364/OPTICA.5.001623. URL <https://opg.optica.org/optica/abstract.cfm?URI=optica-5-12-1623>.
- [13] Patrick Hayden, Debbie W. Leung, and Andreas Winter. Aspects of generic entanglement. *Communications in Mathematical Physics*, 265(1):95–117, Jul 2006. ISSN 1432-0916. doi:10.1007/s00220-006-1535-6. URL <https://doi.org/10.1007/s00220-006-1535-6>.
- [14] Francesco Hoch, Taira Giordani, Nicolò Spagnolo, Andrea Crespi, Roberto Osellame, and Fabio Sciarrino. Characterization of multimode linear optical networks. *Advanced Photonics Nexus*, 2(1):016007, 2023. doi:10.1117/1.AP.N.2.1.016007. URL <https://doi.org/10.1117/1.AP.N.2.1.016007>.
- [15] Kevin Valsón Jacob, Anthony E. Mirasola, Sushovit Adhikari, and Jonathan P. Dowling. Direct characterization of linear and quadratically nonlinear optical systems. *Phys. Rev. A*, 98:052327, Nov 2018. doi:10.1103/PhysRevA.98.052327. URL <https://link.aps.org/doi/10.1103/PhysRevA.98.052327>.
- [16] K G Katamadze, G V Avosopiants, A V Romanova, Yu I Bogdanov, and S P Kulik. Linear optical circuits characterization by means of thermal field correlation measurement. *Laser Physics Letters*, 18(7):075201, may 2021. doi:10.1088/1612-202X/abfc43. URL <https://dx.doi.org/10.1088/1612-202X/abfc43>.
- [17] Nathan Killoran, Thomas R. Bromley, Juan Miguel Arrazola, Maria Schuld, Nicolás Quesada, and Seth Lloyd. Continuous-variable quantum neural networks. *Phys. Rev. Res.*, 1:033063, Oct 2019. doi:10.1103/PhysRevResearch.1.033063. URL <https://link.aps.org/doi/10.1103/PhysRevResearch.1.033063>.
- [18] Plamen Koev and Alan Edelman. The efficient evaluation of the hypergeometric function of a matrix argument. *Mathematics of Computation*, 75(254):833–846, 2006. URL <http://www.jstor.org/stable/4100313>.
- [19] Mario Krenn, Jakob S. Kottmann, Nora Tischler, and Alán Aspuru-Guzik. Conceptual understanding through efficient automated design of quantum optical experiments. *Phys. Rev. X*, 11:031044, Aug 2021. doi:10.1103/PhysRevX.11.031044. URL <https://link.aps.org/doi/10.1103/PhysRevX.11.031044>.
- [20] Chandan Kumar, Ritabrata Sengupta, and Arvind. Optimal characterization of Gaussian channels using photon-number-resolving detectors. *Phys. Rev. A*, 102:012616, Jul 2020. doi:10.1103/PhysRevA.102.012616. URL <https://link.aps.org/doi/10.1103/PhysRevA.102.012616>.
- [21] Sergei Kuzmin, Ivan Dyakonov, and Sergei Kulik. Architecture agnostic algorithm for reconfigurable optical interferometer programming. *Opt. Express*, 29(23):38429–38440, Nov 2021. doi:10.1364/OE.432481. URL <https://opg.optica.org/oe/abstract.cfm?URI=oe-29-23-38429>.
- [22] A. Laing and J. L. O’Brien. Super-stable tomography of any linear optical device. *arXiv preprint arXiv:1208.2868*, 2012.
- [23] Olivier Landon-Cardinal, Luke C. G. Govia, and Aashish A. Clerk. Quantitative tomography for continuous variable quantum systems. *Phys. Rev. Lett.*, 120:090501, Mar 2018. doi:10.1103/PhysRevLett.120.090501. URL <https://link.aps.org/doi/10.1103/PhysRevLett.120.090501>.
- [24] Matthias D. Lang and Carlton M. Caves. Optimal quantum-enhanced interferometry. *Phys. Rev. A*, 90:025802, Aug 2014. doi:10.1103/PhysRevA.90.025802. URL <https://link.aps.org/doi/10.1103/PhysRevA.90.025802>.
- [25] Mirko Lobino, Dmitry Korystov, Connor Kupchak, Eden Figueroa, Barry C. Sanders, and A. I. Lvovsky. Complete characterization of quantum-optical processes. *Science*, 322(5901):563–566, 2008. doi:10.1126/science.1162086. URL <https://www.science.org/doi/abs/10.1126/science.1162086>.
- [26] Lars S. Madsen, Fabian Laudenbach, Mohsen Falamarzi, Askarani, Fabien Rortais, Trevor Vincent, Jacob F. F. Bulmer, Filippo M. Miatto, Leonhard Neuhaus, Lukas G. Helt, Matthew J. Collins, Adriana E. Lita, Thomas Gerrits, Sae Woo Nam, Varun D. Vaidya, Matteo Menotti, Ish Dhand, Zachary Vernon, Nicolás Quesada, and Jonathan Lavoie. Quantum computational advantage with a programmable photonic processor. *Nature*, 606(7912):75–81, Jun 2022. ISSN 1476-4687. doi:10.1038/s41586-022-04725-x. URL <https://doi.org/10.1038/s41586-022-04725-x>.
- [27] R. J. Muirhead. *Aspects of Multivariate Statistical Theory*. Wiley Interscience, 1982.
- [28] M. Poot and H. X. Tang. Characterization of optical quantum circuits using resonant phase shifts. *Applied Physics Letters*, 109(13):131106, 2016. doi:10.1063/1.4962902. URL <https://doi.org/10.1063/1.4962902>.
- [29] Reza Rahimi-Keshari, Artur Scherer, Ady Mann, A T Rezakhani, A I Lvovsky, and Barry C Sanders. Quantum process tomography with coherent states. *New Journal of Physics*, 13(1):013006, jan 2011. doi:10.1088/1367-2630/13/1/013006. URL <https://dx.doi.org/10.1088/1367-2630/13/1/013006>.
- [30] Saleh Rahimi-Keshari, Matthew A. Broome, Robert Fickler, Alessandro Fedrizzi, Timothy C. Ralph, and Andrew G. White. Direct characterization of linear-optical networks. *Opt. Express*, 21(11):13450–13458, Jun 2013. doi:10.1364/OE.21.013450. URL <https://opg.optica.org/oe/abstract.cfm?URI=oe-21-11-13450>.
- [31] Saleh Rahimi-Keshari, Sima Baghbanzadeh, and Carlton M. Caves. In situ characterization of linear-optical networks in randomized boson sampling. *Phys. Rev. A*, 101:043809, Apr 2020. doi:10.1103/PhysRevA.101.043809. URL <https://link.aps.org/doi/10.1103/PhysRevA.101.043809>.
- [32] M. Yu. Saygin, I. V. Kondratyev, I. V. Dyakonov, S. A. Mironov, S. S. Straupe, and S. P. Kulik. Robust architecture for programmable universal unitaries. *Phys. Rev. Lett.*, 124:010501, Jan 2020. doi:10.1103/PhysRevLett.124.010501. URL <https://link.aps.org/doi/10.1103/PhysRevLett.124.010501>.
- [33] A. Serafini. *Quantum Continuous Variables: A Primer of Theoretical* CRC Press, 2017.
- [34] Kunal Sharma, M. Cerezo, Zoë Holmes, Lukasz Cincio, Andrew Sornborger, and Patrick J. Coles. Reformulation of the no-free-lunch theorem for entangled datasets. *Phys. Rev. Lett.*, 128:070501, Feb 2022. doi:10.1103/PhysRevLett.128.070501. URL <https://link.aps.org/doi/10.1103/PhysRevLett.128.070501>.

- [35] Chao Shen, Reinier W. Heeres, Philip Reinhold, Luyao Jiang, Yi-Kai Liu, Robert J. Schoelkopf, and Liang Jiang. Optimized tomography of continuous variable systems using excitation counting. *Phys. Rev. A*, 94:052327, Nov 2016. doi:10.1103/PhysRevA.94.052327. URL <https://link.aps.org/doi/10.1103/PhysRevA.94.052327>.
- [36] Nicolò Spagnolo, Enrico Maiorino, Chiara Vitelli, Marco Bentivegna, Andrea Crespi, Roberta Ramponi, Paolo Mataloni, Roberto Osellame, and Fabio Sciarrino. Learning an unknown transformation via a genetic approach. *Scientific Reports*, 7(1):14316, Oct 2017. ISSN 2045-2322. doi:10.1038/s41598-017-14680-7. URL <https://doi.org/10.1038/s41598-017-14680-7>.
- [37] Si-Hui Tan and Peter P. Rohde. The resurgence of the linear optics quantum interferometer — recent advances and applications. *Reviews in Physics*, 4:100030, 2019. ISSN 2405-4283. doi: <https://doi.org/10.1016/j.revip.2019.100030>. URL <https://www.sciencedirect.com/science/article/pii/S2405428318300431>.
- [38] Yong Siah Teo, Kimin Park, Seongwook Shin, Hyunseok Jeong, and Petr Marek. Highly accurate Gaussian process tomography with geometrical sets of coherent states. *New Journal of Physics*, 23(6):063024, jun 2021. doi:10.1088/1367-2630/abf702. URL <https://dx.doi.org/10.1088/1367-2630/abf702>.
- [39] Max Tillmann, Christian Schmidt, and Philip Walther. On unitary reconstruction of linear optical networks. *Journal of Optics*, 18(11):114002, sep 2016. doi: 10.1088/2040-8978/18/11/114002. URL <https://dx.doi.org/10.1088/2040-8978/18/11/114002>.
- [40] R. Vershynin. *High dimensional probability*. Cambridge University Press, 2018.
- [41] T. J. Volkoff and Yigit Subaşı. Ancilla-free continuous-variable SWAP test. *Quantum*, 6:800, September 2022. ISSN 2521-327X. doi:10.22331/q-2022-09-08-800. URL <https://doi.org/10.22331/q-2022-09-08-800>.
- [42] Tyler Volkoff, Zoë Holmes, and Andrew Sornborger. Universal compiling and (no-)free-lunch theorems for continuous-variable quantum learning. *PRX Quantum*, 2:040327, Nov 2021. doi: 10.1103/PRXQuantum.2.040327. URL <https://link.aps.org/doi/10.1103/PRXQuantum.2.040327>.
- [43] Tyler J. Volkoff. Efficient trainability of linear optical modules in quantum optical neural networks. *Journal of Russian Laser Research*, 42(3):250–260, May 2021. ISSN 1573-8760. doi:10.1007/s10946-021-09958-1. URL <https://doi.org/10.1007/s10946-021-09958-1>.
- [44] Guoming Wang. Property testing of unitary operators. *Phys. Rev. A*, 84:052328, Nov 2011. doi: 10.1103/PhysRevA.84.052328. URL <https://link.aps.org/doi/10.1103/PhysRevA.84.052328>.
- [45] M. Wilde. *Quantum Information Theory*, 2nd Ed. Cambridge University Press, 2017.
- [46] Kazuma Yonezu, Yutaro Enomoto, Takato Yoshida, and Shuntaro Takeda. Universal multi-mode linear optical quantum operation in time domain. In *Frontiers in Optics + Laser Science 2022 (FIO, LS)*, page JTU5A.33. Optica Publishing Group, 2022. doi:10.1364/FIO.2022.JTu5A.33. URL <https://opg.optica.org/abstract.cfm?URI=FiO-2022-JTu5A.33>.
- [47] Xiao-Qi Zhou, Hugo Cable, Rebecca Whittaker, Peter Shadbolt, Jeremy L. O’Brien, and Jonathan C. F. Matthews. Quantum-enhanced tomography of unitary processes. *Optica*, 2(6):510–516, Jun 2015. doi: 10.1364/OPTICA.2.000510. URL <https://opg.optica.org/optica/abstract.cfm?URI=optica-2-6-510>.